Contract Report

High Throughput, Low Toxic Processing of Very Thin, High Efficiency CIGSS Solar Cells

NREL contract no. XXL-5-44205-08, UCF/FSEC Account no. 2012 8098

Year 2, Quarter 3 Report

Report no. FSEC-CR-1707-07

March 2, 2007

Prepared for

National Renewable Energy Laboratory
1617 Cole Boulevard
Golden, CO 80401

Submitted by

Neelkanth G. Dhere
Florida Solar Energy Center®
1679 Clearlake Road
Cocoa, FL 32922-5703

TABLE OF CONTENTS

1: INTRODUCTION

The major concern in the photovoltaic industry is to reduce the cost of PV modules below $1.00/peak watt so as to make the technology economically viable. The research activities at the FSEC PV Materials Lab are focused on developing highly efficient thin-film solar cells capable of being produced using an economical process for achieving this goal. $CuIn_{1-x}Ga_xSe_{2-y}S_y$ (CIGSeS) is a potential candidate for this purpose. Efficiency of 19.5% [1] has been achieved on $CuIn_{1-x}Ga_xSe_2$ (CIGS) solar cell deposited by co-evaporation. Sputtering is the technique capable of providing high yield and high production volume. Research activities presented here focuses on developing CIGSeS thin films by depositing elemental precursor Cu-In-Ga by sputtering technique followed by selenization/sulfurization in either conventional furnace or by rapid thermal processing. During the first year, experiments were carried out to optimize conditions for both conventional and rapid thermal processing approaches. Also experiments were conducted on very thin absorber layers with both the conventional and rapid thermal processing approaches. These initial experiments towards optimizing the selenization parameters were discussed in detail in earlier reports. An efficiency of 11.99% has already been achieved for $CuIn_{1-x}Ga_xS_2$ (CIGS2)_ thin-film solar cells using Cu-rich precursors [2].

2: OPTIMIZATION OF METALLIC PRECURSOR DEPOSITION FOR CIGSeS AND SELENIZATION/SULFURIZATION IN THE CONVENTIONAL FURNACE

Experimental

Optimization of the process parameters is being carried out. In the earlier samples the Cu/(In+Ga) ratio was lower than the desired value of 0.92 - 0.95. Three different indium deposition timings viz., low, intermediate and high were used. The Cu/(In+Ga) ratio for the absorber prepared with intermediate indium deposition timing was ~1. Hence an average of the intermediate and high indium deposition timing was selected. Absorber layers with ~1 μm and 2 μm thicknesses were prepared. Mo-coated glass without the alkali barrier layer was used as a substrate. Moreover, a small amount of NaF was also added during preparation of some of the absorber films. The CIGSeS thin film absorbers were prepared using a two stage process. Stage one involved the deposition of CuGa-In metallic precursors on molybdenum coated soda lime glass substrate. Stage two involved the selenization and sulfurization of the metallic precursors in the DESe and H_2S ambient respectively. The entire elemental stack was selenized or selenized and sulfurized in the temperature range of 475 ºC - 515 ºC. Optical microscopy and scanning electron microscopy (SEM) was carried out to study the morphology of the film. Electron probe micro analysis (EPMA) at NREL and x-ray energy dispersive spectroscopy (XEDS) analysis was carried out to study the chemical composition of the film.

Results and Discussion

Optical Microscopy

The average absorber thicknesses measured using the surface profilometer for the thicker and thinner absorber films were ~2 μm and ~ 1 μm respectively. The optical micrograph (Figure 1) of the ~2 μm thick absorber film reveals micrononuniformity generated during the selenization/sulfurization process. Process parameters are being varied to minimize the micrononuniformity of the CIGSeS film).

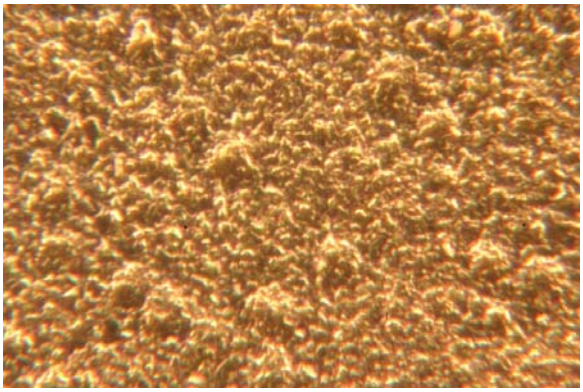

Figure 1: ~2 μm thick absorber film surface

Secondary Electron Microscopy

Figure 2 shows the SEM image of absorber layer prepared at 515^{o}C. The grain size is in the range 1.5 – 2 μm. As can be seen from the figure, there is an uneven grain growth. However, the overall film is compact. Due to the uneven grain growth, surface of the film seems to be porous without deep pores indicating that the absorber is compact in the bulk of the film. Cross sectional SEM of the ~2 μm thick absorber (Figure 4) indicates that the bulk of the film is compact. SEM image of the ~1 μm thick absorber film (Figure 3) reveals a grain size of 0.25 - 0.5 μm and the cross sectional SEM image of the same film (Figure 5) indicates smaller grains at the back of the film and a comparatively open structure in the bulk of the film.

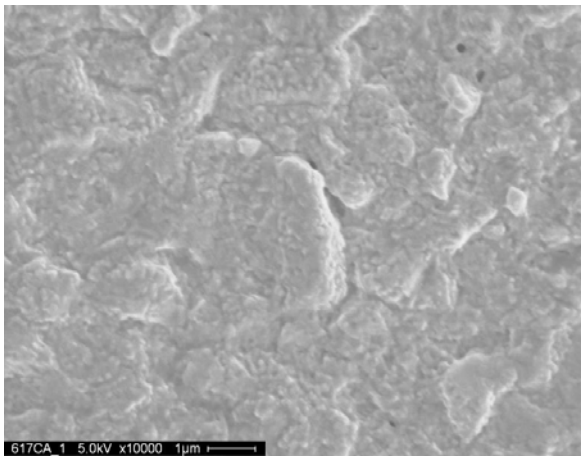

Figure 2: ~2 μm thick absorber film (Sample ID: 617C8A)

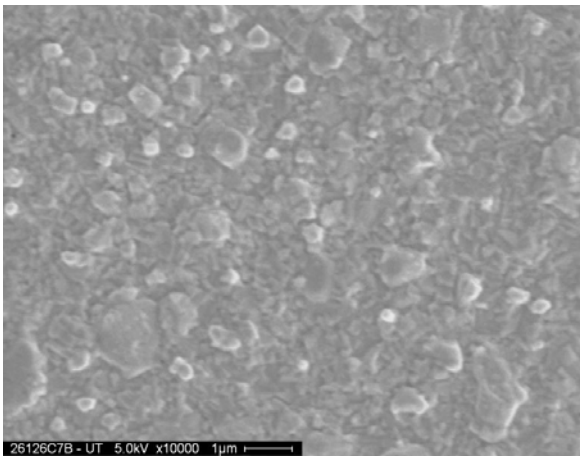

Figure 3: ~1 μm thick absorber film (Sample ID: 26126C7B)

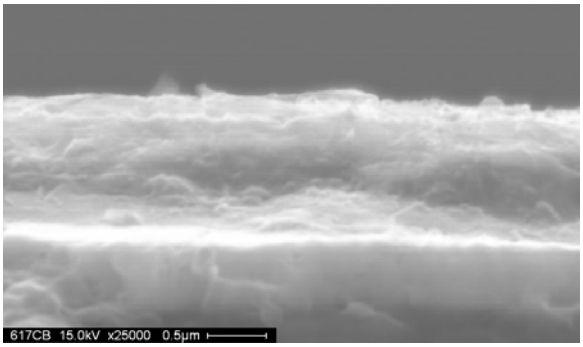

Figure 4: Cross sectional SEM of ~2 µm thick absorber film (Sample ID: 617C8B)

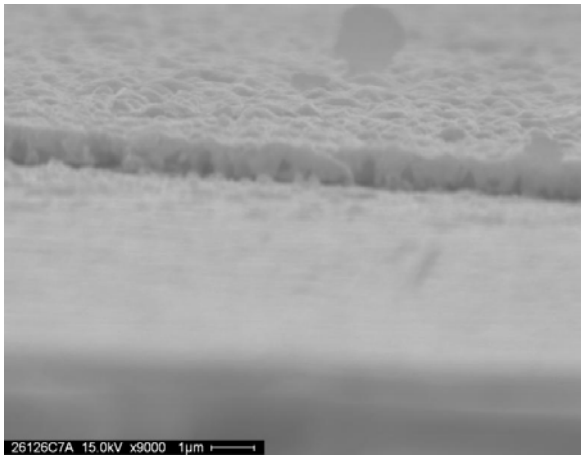

Figure 5: Cross sectional SEM ~ 1 µm thick absorber film (Sample ID: 26126C7A)

Electron Probe Micro Analysis

Cu/(In+Ga) ratios for the 2 µm thick (Sample id: 617C8A and 617C8B) and for the 1 µm thick (Sample id: 2612C7A) absorbers are 0.86 and 1.04 respectively (Table I). The compositions analyzed using electron beam energies of 10 kV and 20 kV corresponded to the near the surface and bulk of the film respectively.

Table I: EPMA at 10 kV and 20 kV, chemical composition of ~ 1 and 2 µm absorber

Sample ID	Voltage	Thickness	Cu	In	Ga	Se	S	Cu/(In+Ga)
			At %					
26126C7A	10 kV	1 µm	21.81	21.91	4.31	32.8	17.18	0.83
617C8A	10 kV	2 µm	23.16	25.78	1.46	30.72	18.85	0.85
617C8B	10 kV	2 µm	22.99	26.87	1.61	22.39	26.13	0.81
26126C7A	20 kV	1 µm	22.59	16.33	5.34	40.56	15.18	1.04
617C8A	20 kV	2 µm	23.77	24.55	3.02	38.19	10.98	0.86
617C8B	20 kV	2 µm	23.85	24.07	3.68	29.09	19.29	0.86

X - Ray Diffraction Analysis

X-ray diffraction pattern of 2- µm and 1- µm thick absorbers provided in Figures 6 and 7 respectively show the growth of chalcopyrite phase of CIGSeS with a = 5.771 nm and c = 11.542 nm (figure 6) and with a = 5.689 nm and c = 11.378 nm (figure 7).Sharper peaks in the XRD pattern indicate larger grain size in the thicker film. Experiments will be carried out to optimize the process parameters in order to enhance the grain growth without affecting the molybdenum back contact.

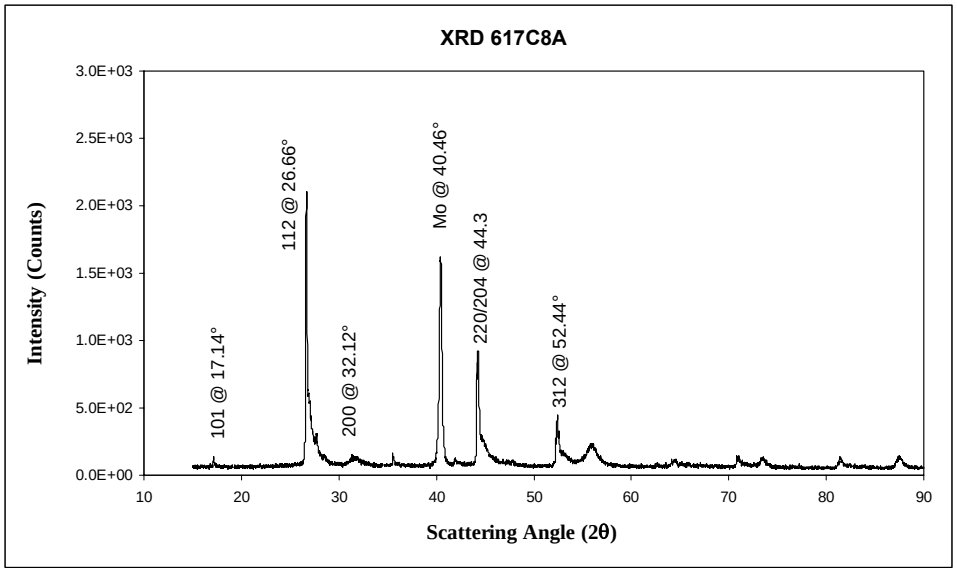

Figure 6: XRD pattern of CIGSeS ~2 µm thick absorber (Sample id: 617C8A)

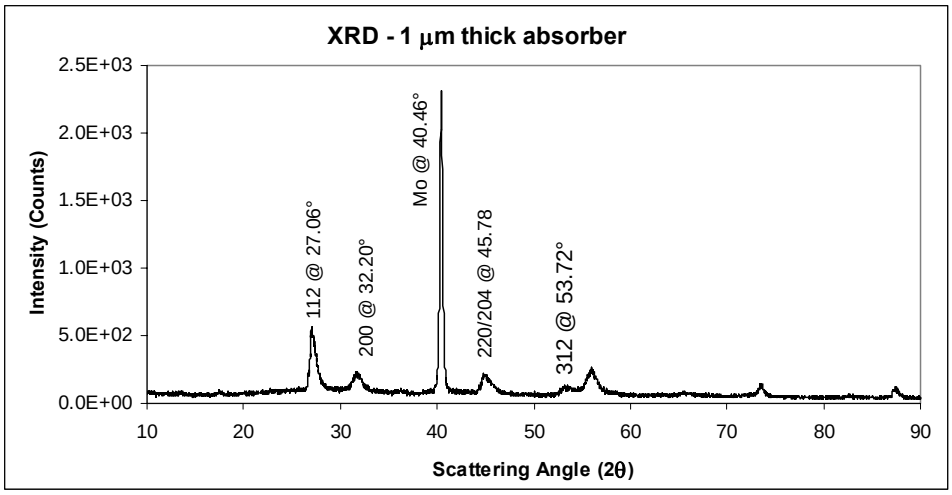

Figure 7: XRD pattern of CIGSeS ~1 μm thick absorber (Sample id: 26126C7A)

3: RAPID THERMAL PROCESSING

Further optimization of the RTP process is being carried out after getting encouraging efficiencies (approaching 13%). Currently experiments are carried out using molybdenum coated soda-lime glass substrates with no sodium-diffusion barrier layer. In the earlier experiments, molybdenum coated soda-lime glass substrates with sodium-diffusion barrier layer were used. Detailed material and photovoltaic characterization is being carried out by optical microscopy, EPMA, XEDS, XRD, SEM and current-voltage (I-V) techniques.

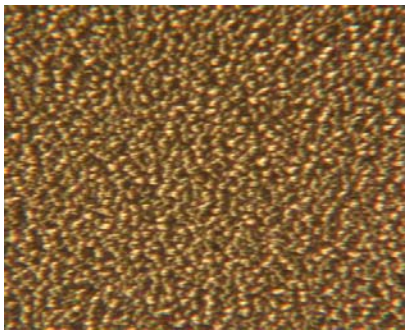

Figure 8: CIGSeS high magnification (1317R21A)

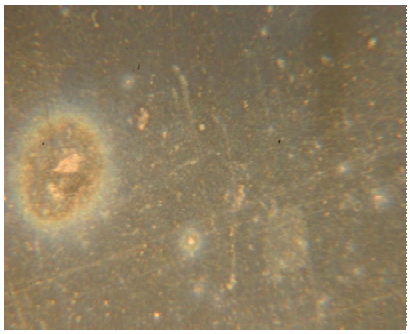

Figure 9: Reacted molybdenum layer (2017R21B)

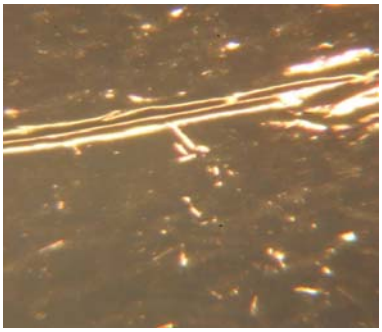

Figure 10: Thermal cracks in molybdenum (2017R21B)

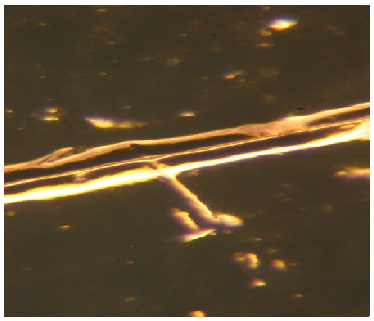

Figure11: thermal cracks in molybdenum (2017R21B)

The optical micrographs reveal various features of the CIGSeS film; most of the film is uniform in appearance as can be seen from figure 8. The molybdenum back contact is getting affected, probably due to reaction with selenium and sulfur (figure 9) and also thermal cracks are

observed in optical micrographs of molybdenum back contacts as examined from the back side through the sodalime glass substrate (Figures 10 and 11).

The scanning electron microscopy results at two different magnifications i.e. 2500X and 5000X are shown in figures 12 and 13; cross-sectional scanning electron microscopy results at magnifications of 18000X and 20000X are shown in figures 14 and 15 respectively.

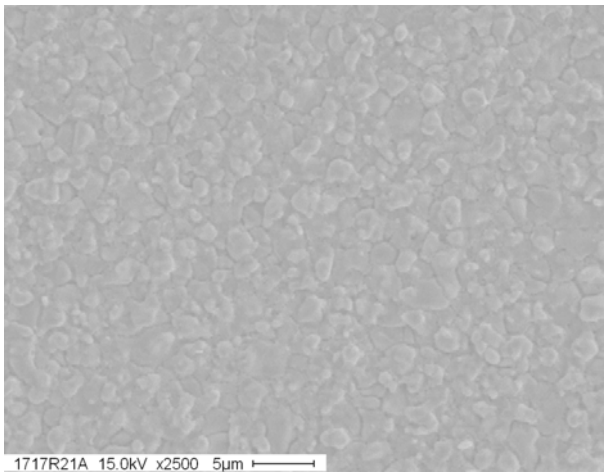

Figure 12: SEM of ~ 2 µm CIGSeS film at 2500X (1717R21A)

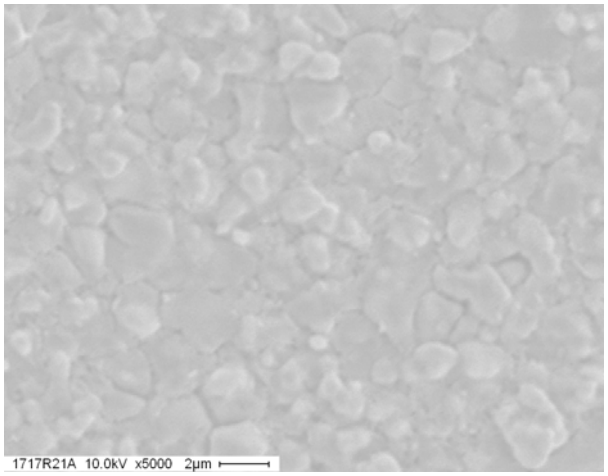

Figure 13: SEM of ~ 2 µm CIGSeS film at 5000X (1717R21A)

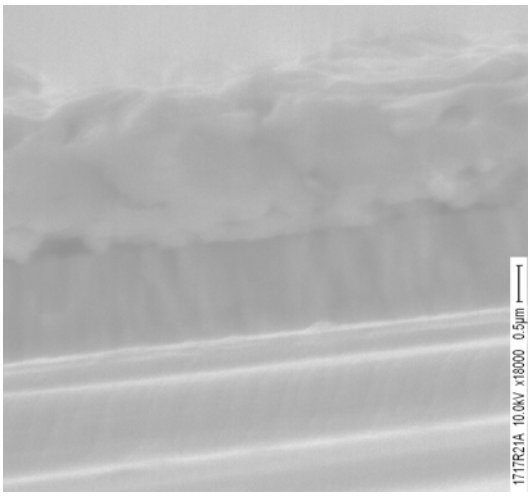

Figure 14: Cross-sectional SEM of CIGSeS µm film at 18000X (1717R21A)

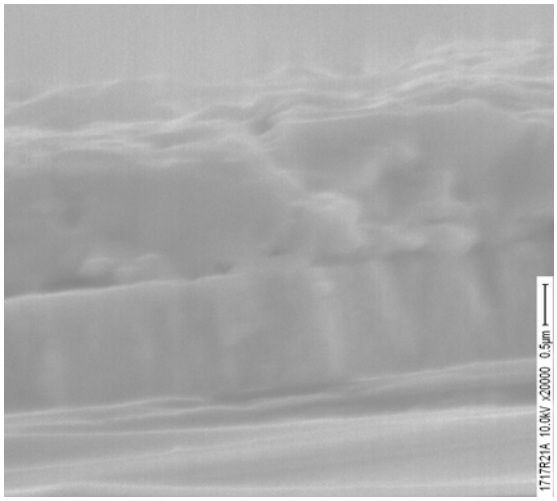

Figure 15: Cross-sectional SEM of ~ 2 CIGSeS film at 20000X (1717R21A)

The SEM micrographs show compactly packed grains with grain size of ~ 2 to 3 microns and the cross-sectional micrographs show CIGSeS film on molybdenum contact with no porosity at the interface, very small gains at the interface are also not observed indicating better grain structure.

Cu/In ratio of approximately 1.09 was obtained from XEDS analysis of CIGSeS film indicating a Cu-rich film (Tables II and III)

Table II: CIGSeS XEDS data.

Element	**Wt %**	**At %**
InL	32.03	23.26
CuK	19.32	25.37
SeK	48.63	51.63

Table III: CIGSeS XEDS data at another location.

Element	**Wt %**	**At %**
InL	33.26	24.17
CuK	20.56	27.00
SeK	46.17	48.8

The EPMA results for the CIGSeS films formed on molybdenum coated soda-lime glass substrates with no diffusion barrier layer are given in Table IV.

Table IV: EPMA analysis data for CIGSeS sample prepared by RTP.

Sample ID	Voltage (kV)	Cu	In	Ga	Se	S	Cu/In+Ga	S/Se+S
1317R21U	10	26.68	22.45	2.35	40.53	7.99	1.08	0.16
1317R21U	20	25.52	22.32	3.78	42.61	5.77	0.98	0.12

Cu/In+Ga ratio is being optimized at ~0.92. As can be seen from the EPMA data the Cu/In+Ga ratio obtained was higher, i.e. 0.9776 instead of the range of 0.92 to 0.95. For the above CIGSeS absorber layer, the indium sputtering time was changed from 41.25 seconds to 5% less, i.e. to 39.4 seconds, rest of the sputtering parameters that is power and pressure were kept same, i.e. 230 watts and 7 x 10^{-4} Torr. As the Cu/In+Ga ratio obtained was higher than required, indium sputtering time was bought back to 41.25 seconds for further experiments.

XRD pattern of sample 1317R21A is shown in figure 16.

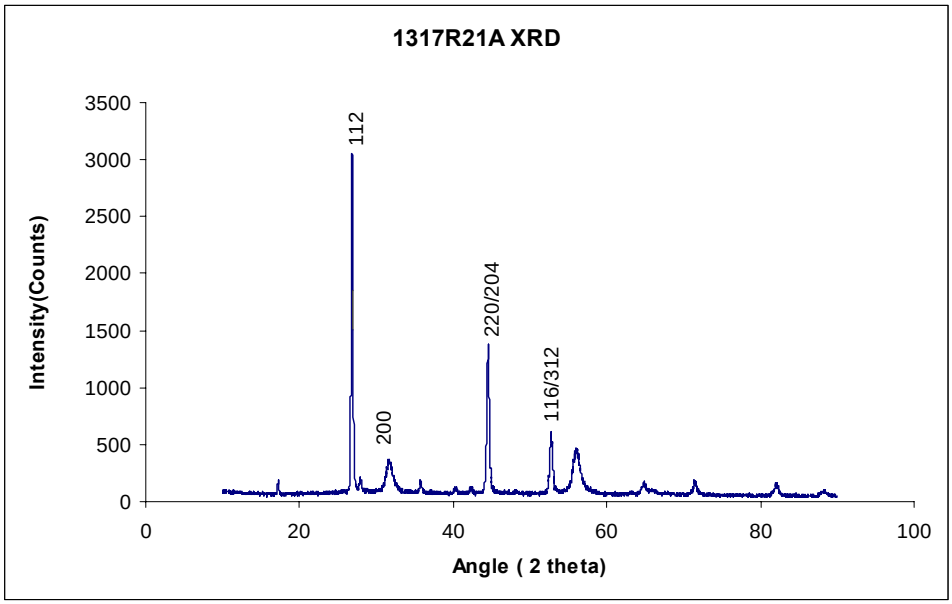

Figure 16: XRD analysis of CIGSeS film.

From the XRD analysis following parameters was calculated: lattice parameter a = 5.758 Å and c = 11.516 Å of the chalcopyrite phase of CIGSeS, giving c/a ratio of 2.000.

Electrical characterization was performed on the cells formed on this absorber layer and the I-V curves were plotted. The PV parameters obtained from this I-V curve are tabulated in Table VI.

Table VI: PV parameters from I-V curve

Sample No.	Cell No.	Cell Area cm^2	V_{oc} mV	I_{sc} mA/cm^2	J_{sc} mA/cm^2	R_s Ω	R_p Ω	FF	η %
1317R21E	01	0.441	400	6.65	15.08	80	700	53	3.2

Due to high series resistance R_s the short circuit current density J_{sc} value is relatively lower; one of the reasons for higher R_s is that molybdenum back contact is getting affected, as can be seen from figures 9,10 and 11.

The thermally affected and cracked molybdenum back contact is also being studied further to improve the series resistance of the cell.

4: EXPERIMENTS ON CIGS2 THIN FILM SOLAR CELLS

Experimental

CIGS2 thin films were prepared in two stages. Stage one involved the deposition of CuGa-In metallic precursors with Cu/(In+Ga) ratio of 1.4 on molybdenum coated glass substrates. Stage two involves the sulfurization of these metallic precursors in dilute H_2S (4-8% H_2S) ambient. The copper rich layer ($Cu_{2-x}S$) that segregated on the surface of near stoichiometric, copper-poor CIGS2 thin film was etched away in a 10% KCN solution. X-ray diffraction (XRD) and Electron Probe Microanalysis (EPMA) were performed at NREL.

Results

X-Ray Diffraction

XRD was carried out on two different samples. Sample 1217SA was expected to have 40% Cu-excess while sample 117SC was expected to have 60% Cu-excess.

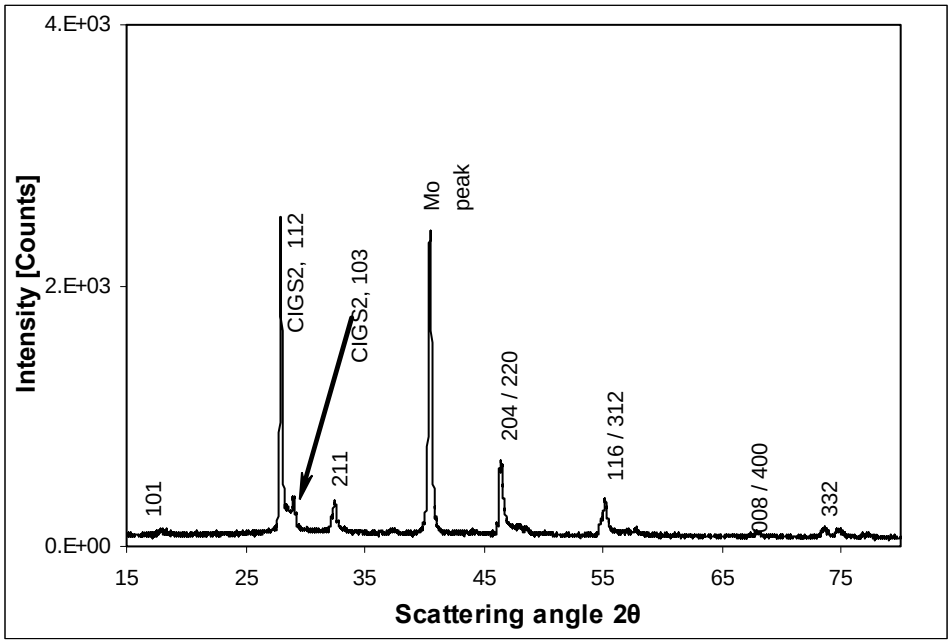

Figure 17: Compound obtained: $CuIn_{0.9}Ga_{0.1}S_2$ and c/a = 2 (sample 1217SA).

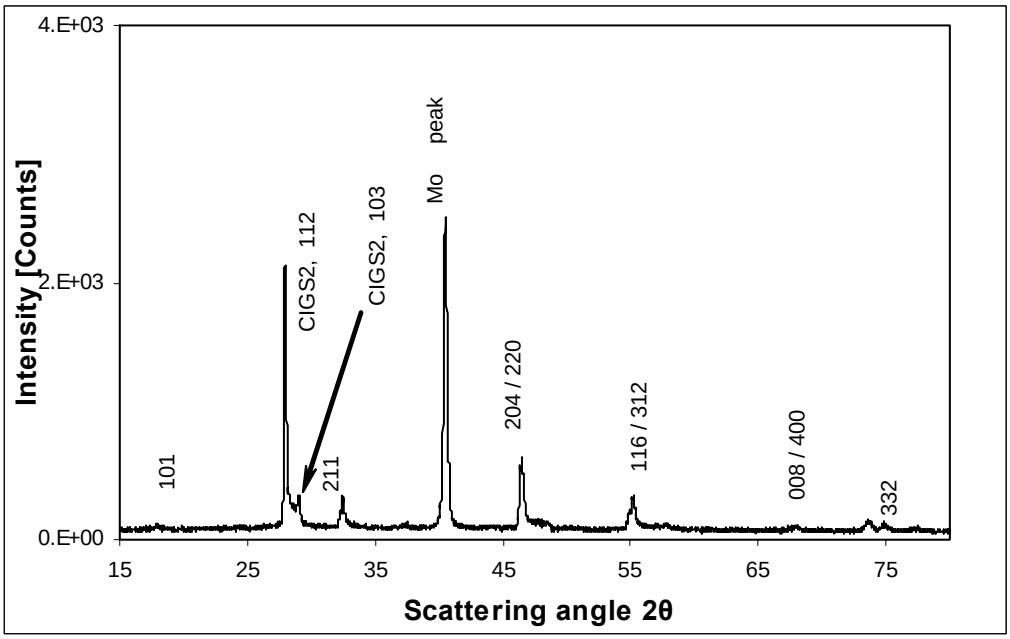

Figure 18: Compound obtained: $CuIn_{0.6}Ga_{0.4}S_2$ and c/a = 2 (sample 117SC).

Electron Probe Microanalysis

Table VII: EPMA results for CIGS2 samples

	10 kV				Cu/In+Ga	**20kV**				Cu/In+Ga
Sample	Cu	In	Ga	S	***Ratio***	Cu	In	Ga	S	***Ratio***
1217SAU (unetched)	39.08	16.6	1.2	43.17	***2.2***	36.29	16.19	3.31	44.19	***1.86***
1217SAE (etched)	23.89	25.7	1.8	48.63	***0.87***					
117SCU (unetched)	39.52	14.5	1	44.99	***2.55***	35.62	16.05	4.08	44.22	***1.77***
117SCE (etched)	23.82	25.8	1.7	48.7	***0.87***	22.97	22.43	5.23	49.35	***0.83***

5: ZnS AND ZnCdS AS ALTERNATIVE BUFFER LAYER FOR CIGS2/CIGSeS SOLAR CELLS

CdS heterojunction partner layer has shown high photovoltaic conversion efficiencies with CIGS absorber layer while efficiencies are lower with $CuIn_{1-x}Ga_xS_2$ (CIGS2) and $CuIn_{1-x}Ga_xS_{2-y}S_y$ (CIGSeS) absorber layers due to high conduction band offset that results in lower values of open circuit voltage and higher interface recombination [4]. Devices with ZnS heterojunction partner layer have shown better blue photon response due to a higher band gap as compared to devices with CdS heterojunction partner layer [4, 5]. Moreover, it has been predicted that lower conduction band offset and higher efficiency may be achieved for cells with alternative buffer layer such as ZnS and ZnCdS. In view of these factors, a study on alternative buffer layers such as ZnS(O,OH) and ZnCdS deposited by chemical bath deposition (CBD) has been initiated at FSEC PV Mat Lab.

Experimental

Currently optimization of concentrations for various chemical reagents is being carried out, and its effect on thickness and composition of film is studied. The substrate used for initial studies was fluorine doped SnO_2 coated soda lime glass. Initially aqueous solution of zinc sulfate/cadmium sulfate was added in an organic solvent and then aqueous solution of ammonium hydroxide and thiourea were subsequently added to the solution. The substrate was then dipped in this solution and reaction was carried out for 45 minutes. Temperature of the solution was maintained at 80° C throughout the process.

Table VIII: Concentration and volume of various chemical reagents used in ZnS/ZnCdS for chemical bath deposition.

	ZnS Deposition		ZnCdS Deposition	
Reagents	**Concentration(M)**	**Amount(ml)**	**Concentration(M)**	**Amount(ml)**
$ZnSO_4$	0.4 M	200 ml	0.08 M	100 ml
$CdSO_4$	-	-	0.0002 M	100 ml
$(NH_2)_2CS$	0.8M	178 ml	0.25 M	178 ml
NH_4OH	9M	22 ml	9 M	22 ml

Results

Auger electron spectroscopy studies confirmed the presence of zinc and sulfur, high concentration of oxygen was also detected in the film. The ZnS(O,OH) film deposited was found to be patchy. Zinc sulfide peaks of ZnS, CdS and ZnCdS were not observed in X-ray diffraction as the film was very thin.

Table IX: Percentage Zn, Cd, S observed in the film by EPMA at 10KV.

Buffer layer	% Zn	% Cd	% S	Cation Anion Ratio
ZnS	58.48	---	41.52	1.41
ZnCdS	21.44	30.44	48.12	1.08

EPMA results (Table IX) showed that the cation to anion ratio is more than unity, which is required for n type buffer layer. To maintain the cation anion ratio near unity during ZnS depositions either thiourea concentration needs to be increased or higher deposition temperature would be required. Further optimization of the CBD parameters will be carried out. This will be followed by characterization of completed CIGSeS/CIGS2 solar cells with ZnS/ZnCdS as the buffer layer.

6: COMPARISON OF CIGS2 SOLAR CELLS BASED ON DEVICE PARAMETERS

A detailed comparative study of two cells having efficiency above 10% was carried out based on the PV parameters measured at NREL and in-house detailed analysis. Efforts have been made to elucidate improvements in PV parameters based on device parameters such as series resistance R_s, shunt resistance R_p, diode factor A, and reverse saturation current density J_o. PV parameters measured under AM1.5 conditions at NREL for the first cell were as follows: V_{oc} = 763.3 mV, J_{sc} = 20.26 mA/cm^2, FF = 67.04% and η = 10.4% [3] and for the second cell were as follows: V_{oc} = 830.5 mV, J_{sc} = 20.88 mA/cm^2, FF = 69.13% and η = 11.99% [2]. The current-voltage (I-V) characteristics of these two cells are shown in figure 19. Although the areas of these two cells are slightly different, as the analysis is carried out using current density values, this area difference is taken into consideration.

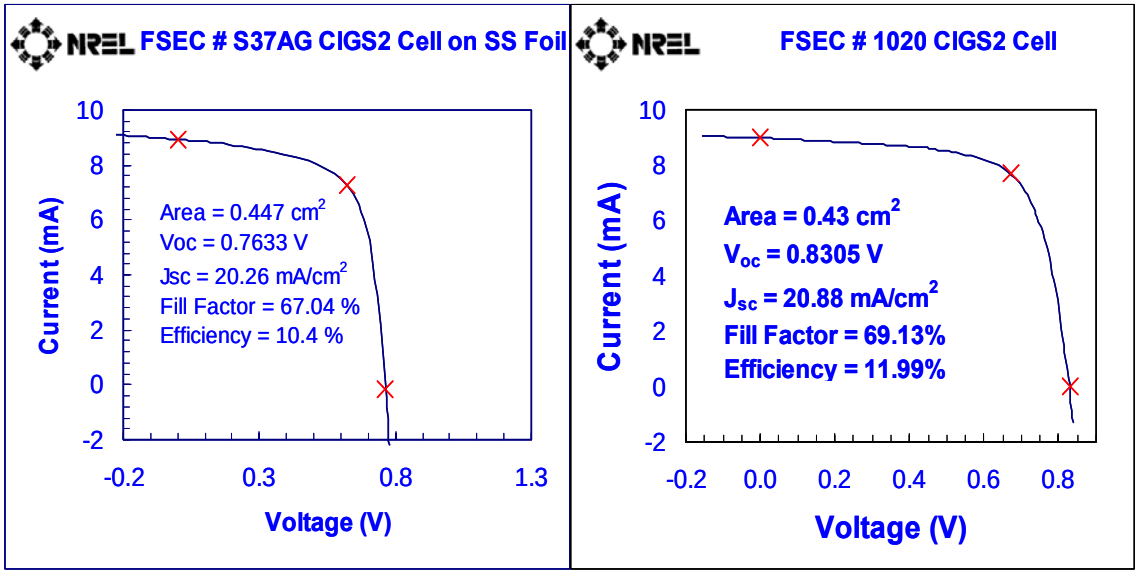

Figure 19: I-V Characteristics of the two solar cells

Results of the detailed PV characteristics consisting of the analysis of short circuit current density, J versus voltage, V obtained at NREL are presented in the following. The J-V characteristics in light and dark were compared to verify if the light characteristic was essentially a translated curve with light short circuit current, J_{sc} or J_L. The J-V characteristics in light and dark for 10.4%and 11.99% cell are shown in figure 20 and 21 respectively. As can be seen from

figure 20 there is a slight crossover at higher current densities which suggests moderately photoconducting heterojunction partner layer.

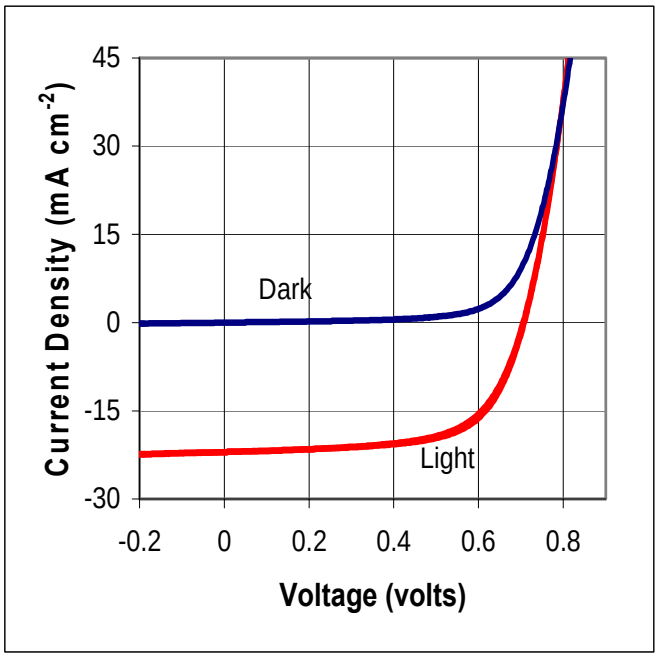

Figure 20: Variation of light and dark current densities with voltage for 10.4% cell

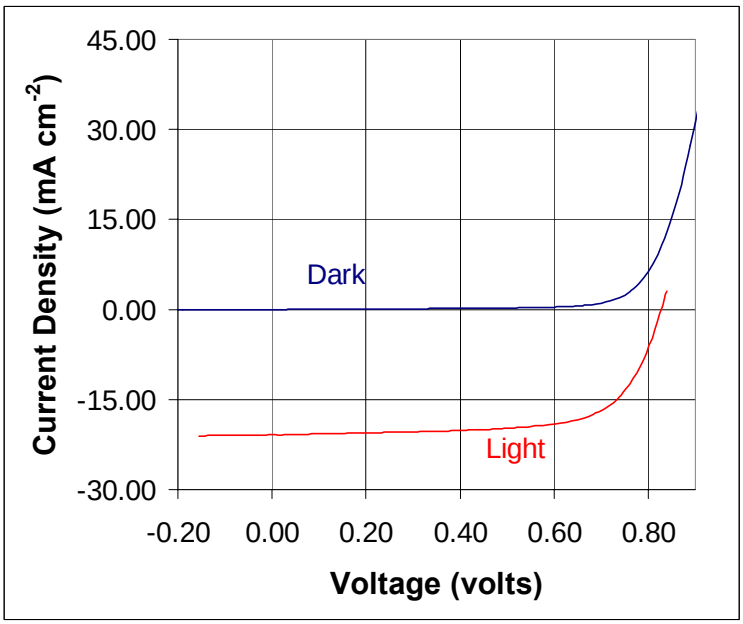

Figure 21: Variation of light and dark current densities with voltage for 11.99% cell.

From the J-V characteristics, a plot of dJ/dV versus V curve was plotted for both cells. These plots are shown in figure 22 and 23 for 10.4% and 11.99% cell respectively. This dJ/dV versus V curve measures the ac conductance around the J_{sc} point. The dark curve gives a shunt resistance R_p value of 1160 Ω cm^2 for the 10.4% cell while shunt resistance R_p values of 1225 Ω cm^2 under illumination and 2500 Ω cm^2 in dark were calculated for 11.99% cell.

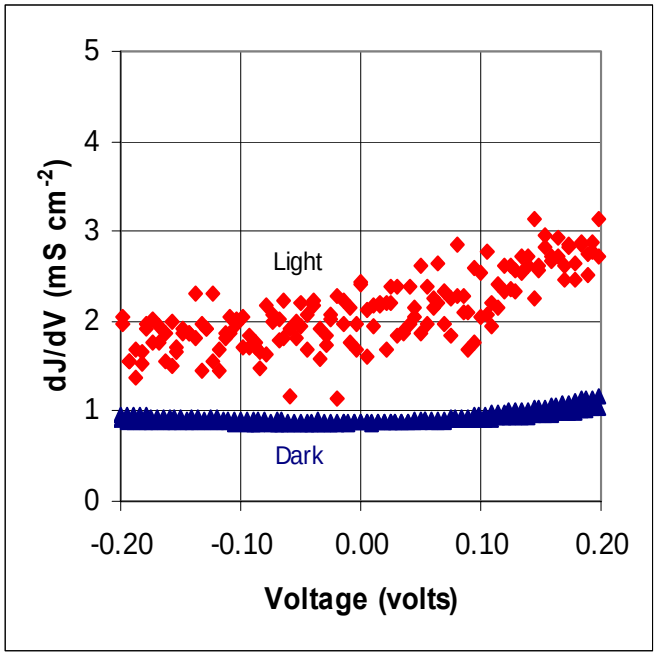

Figure 22: dJ/dV versus voltage characteristics for 10.4% cell

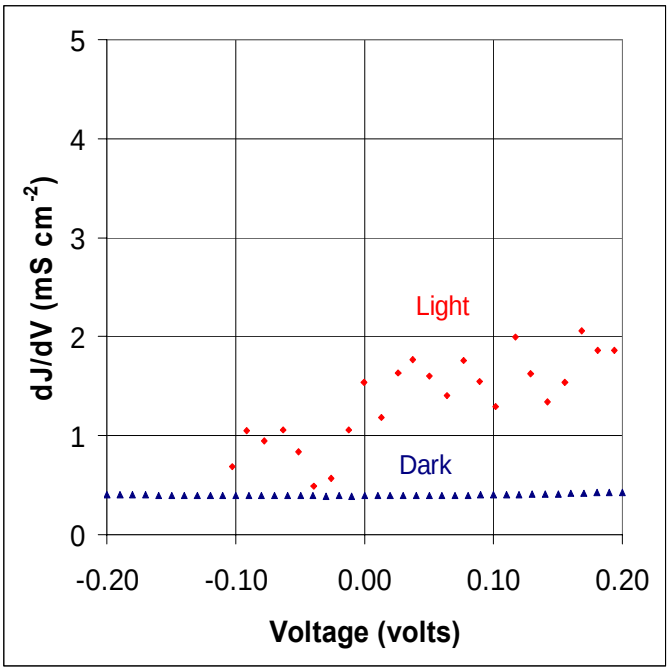

Figure 23: dJ/dV versus voltage characteristics for 11.99% cell

The dV/dJ versus [1- (dV/(dJR$_p$)]/[J+J$_{sc}$ + (V/R$_p$)] curve was plotted to estimate ac resistance under forward bias. Earlier dV/dJ versus 1/[J$_o$+J$_{sc}$] curve was plotted which showed a slightly larger divergence. Hence a correction was made by using a more complex function [1-(dV/(dJR$_p$)]/[J+J$_{sc}$ + (V/R$_p$)] that accounts for the current lost across the shunt resistance, R$_p$. This curve for the two cells is shown in figures 24 and 25.As can be seen from figures 24 and 25 the curves are straight lines that indicate diode or exponential behavior. The series resistance R$_s$, can be found out by extrapolating the curve to ∞ current. It was found out that the R$_s$ values were ~0.6 Ω cm^2 for the 10.4% cell and is in the range of 0.2-0.6 Ω cm^2 under illumination and 1.15 Ω cm^2 in dark for the 11.99% cell.

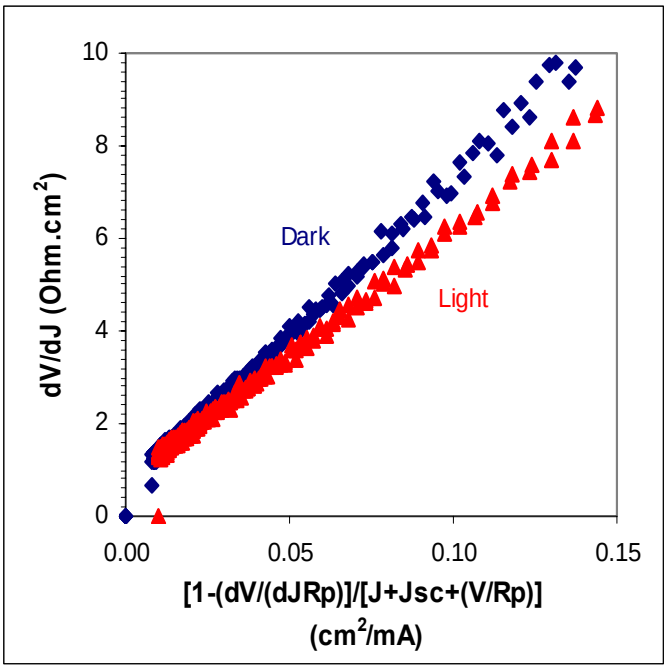

Figure 24: Variation of dV/dJ with $[1-(dV/dJR_p)]/[J+J_{sc}+(V/R_p)]$ for 10.4% cell

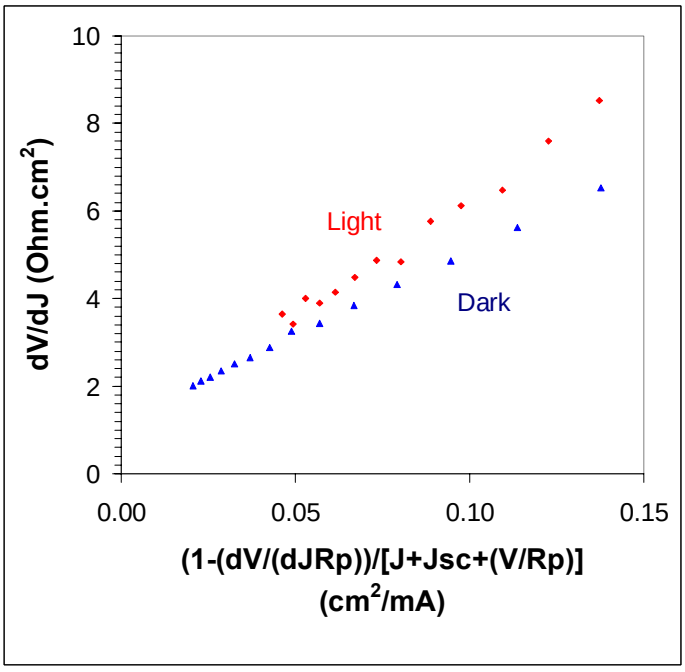

Figure 25: Variation of dV/dJ with $[1-(dV/dJR_p)]/[J+J_{sc}+(V/R_p)]$ for 11.99% cell

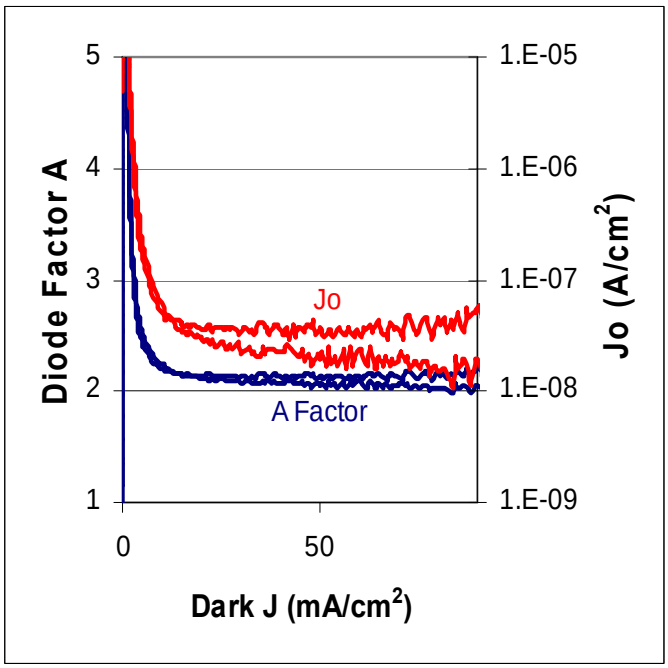

Figure 26: Variation of diode factor, A and reverse saturation current density, J_o with the dark current density, J for 10.4% cell.

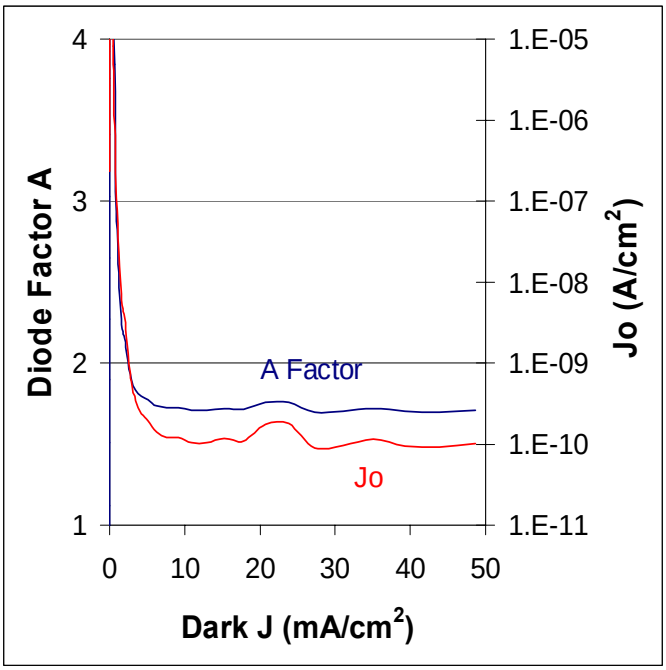

Figure 27: Variation of diode factor, A and reverse saturation current density, J_o with the dark current density, J for 11.99% cell.

Values of the diode factor, A and reverse saturation current density, J_o can be obtained from a plot of natural logarithm of ($J+J_{sc}$) versus corrected voltage V' i.e. (V-RsJ). Figures 26 and 27 show a plot of the diode factor, A and reverse saturation current, J_o versus ln [J (dark)] for the two cells. For the 10.4% cell the diode factor A is ~2.1 and reverse saturation current density J_o is ~2.6×10^{-8} A cm^{-2} for a wide range of dark current densities. Similarly for the 11.99% cell the diode factor A is ~1.72 and reverse saturation current density Jo is ~1.41×10^{-10} A cm^{-2}.

It can be seen from these values that there is an improvement in the series and shunt resistance and the diode factor. Moreover, there is a significant reduction in the reverse saturation current density resulting in higher voltages for the 11.99% cell.

7: REFERENCES

[1] Miguel A. Contreras, K. Ramanathan, J. AbuShama, F. Hasoon, D. L. Young, B. Egaas and R. Noufi, Prog. Photovolt: Res. Appl. 2005; 13:209–216.

[2] Anant H. Jahagirdar and Neelkanth G. Dhere, Proceedings of the 4th IEEE World Conference of Photovoltaic Energy Conversion, Hawaii, 2006.

[3] Neelkanth G. Dhere, Shashank R. Kulkarni, and Shantinath R. Ghongadi, Proc. 28th IEEE Photovoltaic Specialists' Conference, Anchorage, Alaska, Sept. 15-22, 2000.

[4] M.A.Contreras, T.Nakada, M.Hongo, A.O.Pudov, J.R.Sites 3rd World Conference on Photovoltaic Energy Conversion, Osaka, Japan, May 2003.

[5] R.N.Bhattacharya, K.Ramanathan, L.Gedvilas,B., Journal of Physics and Chemistry of Solids 66(2005) 1862–1864.